Journal of Physics B: Atomic, Molecular and Optical Physics

Calculated electron impact ionisation fragmentation patterns

OPEN ACCESS
IOP Publishing
Journal of Physics B: Atomic, Molecular and Optical Physics
J. Phys. B: At. Mol. Opt. Phys. **54** (2021) 235203 (12pp)
https://doi.org/10.1088/1361-6455/ac42db

Calculated electron impact ionisation fragmentation patterns

Vincent Graves[1,2], **Bridgette Cooper**[1] and **Jonathan Tennyson**[1,*]

[1] Department of Physics and Astronomy, University College London, London WC1E 6BT, United Kingdom
[2] School of Physical Sciences, The Open University, Walton Hall, Milton Keynes MK7 6AA, United Kingdom

E-mail: j.tennyson@ucl.ac.uk

Received 26 September 2021, revised 29 November 2021
Accepted for publication 14 December 2021
Published 10 February 2022

Abstract

There are many measurements and calculations of total electron impact ionisation cross sections. However, many applications, particularly in plasma physics, also require fragmentation patterns. Approximate methods of deducing partial cross sections are tested based on the use of total cross section computed within the well-used binary encounter Bethe approximation. Partial ionisation cross sections for three series of molecules including CH_4, CF_4 and CCl_4; SiH_4 and $SiCl_4$; NH_3 and PH_3, were estimated using two methods. Method one is semi-empirical and uses mass spectroscopy data to fix the partial cross sections at a single electron energy. The second is a fully computational method proposed by Huber *et al* (2019 *J. Chem. Phys.* **150** 024306). Comparisons with experimental results suggest that the mass spectroscopy method is more accurate. However, as Huber's method requires no experimental input, this method could be used as a first approximation when no experimental data is available. As mass spectroscopy sometimes provides incomplete datasets, a hybrid method based on the use of both methods is also explored.

Keywords: electron impact ionisation, branching ratios, binary encouter born

(Some figures may appear in colour only in the online journal)

1. Introduction

Electron impact ionisation cross sections have importance in many areas of science including astrophysics and astrochemistry [1], plasma sciences [2–5] and environmental sciences [6, 7]. The wide scope of applications has led to electron impact ionisation cross sections being extensively studied, both experimentally and computationally. Theoretically, a number of empirically motivated models are available for predicting total ionisation cross sections such as the Binary Encounter Bethe (BEB) method proposed by Kim and Rudd [8], the Deutsch–Märk [9] (DM) method and the spherical complex optical potential [10] method. These have been extensively used to calculate the total ionisation cross sections of atoms, molecules, ions, radicals and clusters with generally successful outcomes [11, 12]. In a previous paper by the authors [13] improvements to the computational total cross section using the BEB method were investigated by using effective core potential (ECP) basis sets as well as using a semi-empirical polarizability scaling factor, αBEB. An ECP basis set differs from a non-ECP basis set through the use of an effective potential which replaces the core electrons. ECPs can improve the description of relativistic effects in heavy atoms, which in turn improve the representation of the valence orbitals. However, use of an ECP means the ionisation of the inner electrons is no longer modelled, resulting in an underestimation of ionisation cross sections at high energy.

* Author to whom any correspondence should be addressed.

While total electron impact ionisation cross sections are useful, often, it is desirable to know the cross sections of the dissociation products due to ionisation. These can be represented as the total cross section multiplied by a branching ratio for the production of a given species. Such branching ratios are measured, usually at a single electron collision energy, by mass spectroscopy experiments or in specialist experiments designed specifically to study fragmentation patterns [14–20]. These experiments often provide only relative cross sections but they can then be made absolute using BEB or similar procedures [21]. However, there are many cases where measured branching ratios do not exist as a function of electron collision energy; for these it would be desirable to have a reliable theoretical procedure for predicting them. This is particularly true for studies of radicals and energetically unstable species which are of importance in many plasmas but are difficult to study experimentally.

Computational techniques do exist for predicting fragmentation patterns, but these can be very resource demanding and take considerable time to compute. One such technique is the Rice–Ramsperger–Kassel–Marcus (RRKM) theory which uses the potential energy surface of the molecule to compute rate constants and branching ratios [22]. Here, two simplified methods for producing partial ionisation cross sections are considered. These are designed to provide estimated, energy-dependent fragmentation patterns when no direct experimental data is available. The molecules studied are relatively simple but many are used in important industrial applications [1, 3, 4, 23–27], they include: CH_4, CF_4 and CCl_4; SiH_4 and $SiCl_4$; NH_3 and PH_3.

One method, referred to as the mass spectrum derived throughout this work, uses relative data from mass spectra obtained at a single electron impact energy to provide energy-dependent branching ratios [28]. The National Institute of Standards and Technology (NIST) provides an open, easily accessible and extensive database of experimental mass spectra which we use here [29]. These mass spectra were determined using electron ionisation gas chromatography-tandem mass spectrometry. The database contains a series of small molecules and peptides. This method was originally proposed by Hamilton *et al* [28] and used a correction introduced via the BEB method, shown in section 2.2, to compensate for the different dissociation thresholds of the fragments and to produce fragment cross sections that are energy dependent.

Mass spectra were also used by Irikura [30] for the determination of fragmentation ratios of organic compounds potentially found on the surface of Mars, as sampled by the *curiosity* rover. The *curiosity* rover used a known internal calibrant, CO_2, and produced partial ionisation cross sections using *in situ* mass spectrum data. However, in this case no attempt was made to predict the energy dependence of the fragmentation patterns.

The second method requires no experimental input and was first proposed by Huber *et al* [31]. This method, referred to as Huber's method below, uses a calculated dissociation threshold to get a branching ratio approximation which is corrected for energy dependence. Finally, we test a hybrid method which uses Huber's method to produce branching ratios for any desired fragments not observed in the experimental mass spectrum.

The following section 2 expands on the methods used for the computation of the partial and total ionisation cross sections, with section 3 containing the computational details. Finally, section 4 contains computed cross sections of the seven molecules studied with comparisons to experimental details.

2. Method

2.1. Total ionisation cross section

In this work, partial ionisation cross sections are produced by imposing branching ratios onto total ionisation cross sections determined through the use of the BEB method [8], shown in equation (1)

$$\sigma_{\mathrm{BEB}} = \frac{S}{t+u+1}\left[\frac{\ln t}{2}\left(1-\frac{1}{t^2}\right)+1-\frac{1}{t}-\frac{\ln t}{t+1}\right]. \quad (1)$$

Here, $S = 4\pi a_0^2 N(R/B)^2$, with a_0 the Bohr radius, R the Rydberg energy, N the orbital occupation, B the binding energy, $t = T/B$ where T is the energy of the incoming electron, and $u = U/B$ where U is the orbital kinetic energy. The total cross section is found by summing the BEB cross sections for each of the occupied orbitals in an atom or molecule. A key feature of this method is that it does not require fitting parameters and can be used when the dipole oscillator strengths are not known. This makes the method extremely flexible for estimating ionisation cross sections as the only parameters required are the occupation numbers, binding energy and kinetic energies of each of the orbitals, all of which can be obtained through a Hartree–Fock calculation.

The BEB approach inherently treats single ionisation. However, in a similar approach to Nishimura *et al* [32], we assume that Auger processes are likely to double the ionisation cross section for ionisation from molecular orbitals that have a binding energy greater than the double ionisation threshold.

2.2. Branching ratios

We compare two methods for producing the branching ratios used in the determination of the partial cross sections. The first method, discussed in section 2.3, relies on the use of experimental mass spectrum data. The second method, discussed in section 2.4, uses Huber's method and thus is solely computational and predictive. If the MSD method does not provide all of the fragmentation patterns desired then Huber's method can be used to provide information on the missing fragments giving a hybrid method which contains all of the fragmentation information desired.

A crucial requirement of the definition of the calculated branching ratios is that they should sum to unity and should be zero when the energy of the colliding electron (T) is below the threshold of the dissociation pathway

$$\Gamma_i(T) = \begin{cases} \dfrac{b_i}{\sum_j^n b_j} & T \geqslant D_i \\ 0 & T < D_i, \end{cases} \quad (2)$$

where, D_i is the appearance threshold of species i due to break-up (dissociation) of the parent ion, Γ_i is the branching ratio of species i and b_i is some intensity value of species i and n is the number of possible pathways.

In this work we estimate partial ionisation cross sections by multiplying the BEB total ionisation cross section with the respective branching ratio as

$$\sigma_i(T) = \Gamma_i(T)\sigma_{\mathrm{BEB}}(T). \tag{3}$$

The threshold for the formation of each fragment must be aligned with the ionisation threshold plus the appropriate dissociation energy in case of fragmentation of the parent ion. Hamilton *et al* [28] proposed modifying the BEB method to include the dissociation thresholds directly within the BEB model by adjusting the value of t to give t_i for each fragmentation process considered

$$t_i = \left(\frac{T}{B - D_i}\right). \tag{4}$$

However, this is not used here. Instead, branching ratios were used to obtain the energy dependency of the partial cross sections. Only the BEB of the parent molecule was used.

2.3. Mass spectrum method

Experimental mass spectra can be used to determine the branching ratios at a given energy using equation (2). In this case b_i represents the intensity of the species i at the energy at which the measurement was taken. The intensities for each fragment was taken using the most abundant isotopologue and not corrected for isotopic abundances, although this could be done.

Usually the mass spectrum only defines the branching ratio at a single electron impact energy (T^{ref}). In the MSD method the ratio can be made energy dependent using

$$\Gamma_i(T) = \begin{cases} 0 & T < D_i \\ \Gamma_i(T^{\mathrm{ref}})\left[1 - \left(\frac{D_i}{T}\right)^{\gamma}\right] & T \geqslant D_i. \end{cases} \tag{5}$$

This equation is only strictly valid if we assume that the known branching ratios are the asymptotic branching ratios, that is as T goes to infinity, the branching ratio goes to the known branching ratio which equivalent to assuming $T^{\mathrm{ref}} = \infty$. This means that when we take the known branching ratios at a finite reference energy, we do not reproduce the known branching ratios at that reference energy. However, the error is often less than 15% for the main fragments. The error will increase the lower the reference energy is, and also the closer the highest threshold is to the reference energy. That is we are making the assumption when we are using these equations that the reference energy is sufficiently high that all channels are open, and that the branching ratios are all stable.

The value of γ in equation (5) is used to control how quickly the asymptotic value of Γ_i is reached. It was determined to be 1.5 ± 0.2 by Janev and Reiter [33]. The value of 1.5 was adopted in this work. There are many ways that the energy dependency could have been included. A result of using this method is that the energy-dependence for each fragment is a smooth monotonic function, which, when combined with the smooth BEB cross sections, results in partial cross sections that are all smooth curves. We note the recent study by Amorim *et al* [34] found some variation of the shape of the fragmentation curves as function of energy but at present we have no means of predicting this behaviour.

The mass spectra used were taken from the openly accessible NIST Mass Spectral Library [29]. However these datasets do not give an energy at which the spectra were taken. An older version of the manual [35] gives a value of 70 eV so we assumed this value is true for all spectra. Due to the experimental method used for the measurement of some molecules, not all fragments are present in the spectra and there may be other issues with the detection of certain (particularly light) fragments. The branching ratios of missing fragments can be estimated using Huber's method outlined below.

2.4. Huber's method

Huber *et al* [31] outlined a method for the determination of branching ratios for diatomic molecules. At threshold, Huber *et al* proposed a relationship between the dissociation threshold for the formation of a fragment from the parent ion and the branching ratio:

$$b_i = \left(\frac{1}{D_i}\right)^{\beta}, \tag{6}$$

where β was determined to be 3 by Huber *et al* [31, 36] through comparison with experimental branching ratios. β is not energy dependent. The value b_i can then be used in equation (2) to determine the branching ratio. The energy dependence of these branching ratios is then determined using equation (5); this allows for an estimation of the branching ratio at energies above the various dissociation thresholds. Finally, the branching ratios are normalised to satisfy equation (2).

Huber *et al* [31] also proposed the addition of a so called structural factor, ζ, which allows for other processes not included within the threshold approximation:

$$\Gamma'_i = \Gamma_i(T)\zeta_i, \tag{7}$$

where Γ' is the real branching ratio. The value ζ can most easily be determined from the experimental branching ratio using

$$\zeta_i = \frac{\Gamma_i^{\mathrm{exp}}}{\Gamma_i(T)}, \tag{8}$$

where the superscript 'exp' represents experimental data. It has been observed that for the dissociation of single C–H bonds, $\zeta \leqslant 1$ and for more complex dissociation, $\zeta > 1$ [31]. Here we assume $\zeta = 1$ but note that other values could be explored in a future implementation of our methodology.

2.5. Fragment selection process

The selection of the possible fragments from the target molecule is an important step in Huber's method. The model,

as proposed by Huber *et al*, included the fragmentation pathways:

$$\mathrm{AB} + \mathrm{e}^- \rightarrow \mathrm{AB}^+ + 2\mathrm{e}^-$$
$$\mathrm{AB}^+ + 2\mathrm{e}^- \rightarrow \mathrm{A}^+ + \mathrm{B} + 2\mathrm{e}^-$$

or,

$$\mathrm{AB}^+ + 2\mathrm{e}^- \rightarrow \mathrm{A} + \mathrm{B}^+ + 2\mathrm{e}^-,$$

where AB is an arbitrary molecule. The dissociation pathways presented are assumed to be barrierless as they depend only on the dissociation energy (see equation (6)) of the particular pathway.

For polyatomic species, there are often multiple fragmentation pathways [37], resulting in the same ionic fragments. This is particularly true for light fragments, for example in the break up of methane, CH_4, the fragment H^+ could form as a result of breaking one to four bonds:

$$\mathrm{CH_4} + \mathrm{e}^- \rightarrow \mathrm{H}^+ + \mathrm{CH_3} + 2\mathrm{e}^-$$
$$\mathrm{CH_4} + \mathrm{e}^- \rightarrow \mathrm{H}^+ + \mathrm{H} + \mathrm{CH_2} + 2\mathrm{e}^-$$
$$\mathrm{CH_4} + \mathrm{e}^- \rightarrow \mathrm{H}^+ + 2\mathrm{H} + \mathrm{CH} + 2\mathrm{e}^-$$
$$\mathrm{CH_4} + \mathrm{e}^- \rightarrow \mathrm{H}^+ + 3\mathrm{H} + \mathrm{C} + 2\mathrm{e}^-.$$

In the Huber model only the lowest energy pathway is included, for example the dissociation energy resulting $H^+ + CH_3$ is used for the H^+ threshold. This is usually the pathway with the fewest number of bond breaks. All of the molecules studied here contain several atoms of the same element, which means that the formation of ions of that element can occur through one or multiple bond breaks, such as the case above.

The threshold approximation cannot accurately model the formation of molecular ions that are not the result of simple bond breaking in the parent ion. For example, the formation of H_2^+ or H_3^+ from CH_4 requires the formation of new bond(s) which do not appear in the target. As the formation of these fragments relies on processes such as post-ionisation collisions and/or complicated transition states, these pathways are not considered in the model used here, as the branching ratio will not depend on the energetics of the resulting fragments alone.

Pathways arising from double ionisation of the parent ion are not included in the model. In double ionisation process, the fragmentation would be influenced by the Coulombic repulsion of the two positive charges making fragmentation more likely. However, as the value for β above was not found to be energy dependent by Huber *et al*, this suggests that the formation of, for example, A^+, through double ionisation is insignificant.

3. Computational details

3.1. Total ionisation cross sections

Total ionisation cross sections were determined using the BEB method as implemented in quantemol electron collisions (QEC) version 1.2 [38]. QEC is a graphical user interface that uses MOLPRO [39] to perform the necessary target calculations. It is worth noting that although the BEB method is used in this work, the branching ratio equations can be applied to any total ionisation cross section, observed or calculated. All calculations below used Gaussian type orbital cc-pVDZ [40] basis sets which were previously found adequate to give converged BEB results [13]. For CCl_4 and $SiCl_4$ an ECP basis set was used: ECP10MWB [41] on the Si and Cl and ECP2MWB on the C. These core potential basis sets were chosen after an extensive investigation into the effect of ECPs on the total ionisation cross section [13]. Initial geometries were obtained from the Computational Chemistry Comparison and Benchmark DataBase (CCCBDB) [42]. Geometries were re-optimised within QEC. QEC provides the option to specify an experimental ionisation threshold which is then used in the calculation, however, the default is to use Koopmans' theorem [43] which allows for the ionisation potential (IP) to be replaced with the binding energy of the highest occupied molecular orbital. Use of Koopmans' theorem has been shown to provide a reliable estimate of the effective ionisation threshold and it was adopted here. In our model, the formation of the parent ion was assumed to determine the IP.

Table 1. The calculated dissociation thresholds (D_i) and experimental AE [44] of CH_4 in eV.

Ion	AE (eV)	D_i (eV)
CH_4^+	15.00	14.86
CH_3^+	15.00	14.76
CH_2^+	17.00	19.26
CH^+	25.00	24.33
C^+	30.00	29.50
H^+	25.00	19.24

3.2. Dissociation thresholds

The balance between computer time and the accurate calculation of the dissociation thresholds of the relevant ions was investigated. Using MOLPRO it was found that satisfactory results could be generated relatively quickly using the couple-cluster method at the CCSD(T) level using Dunning's basis set cc-pVQZ [40], where possible or reducing to cc-pVTZ, or cc-pVDZ when necessary. The formation threshold, D_i, for each fragment, i.e. where the onset of dissociation occurs, was determined using the pathway and equation as shown below for an arbitrary molecule AB to form A^+,

$$\mathrm{AB} + \mathrm{e}^- \rightarrow \mathrm{A}^+ + \mathrm{B} + 2\mathrm{e}^-$$

$$D_{\mathrm{A}^+} = E(\mathrm{A}^+) + E(\mathrm{B}) - E(\mathrm{AB}^+) + \mathrm{IP}, \qquad (9)$$

where $E(X)$ is the energy of species X. These thresholds were corrected for basis set superposition error using a counterpoise correction.

To ensure the fragment thresholds determined here were in line with the total ionisation cross section threshold, they were

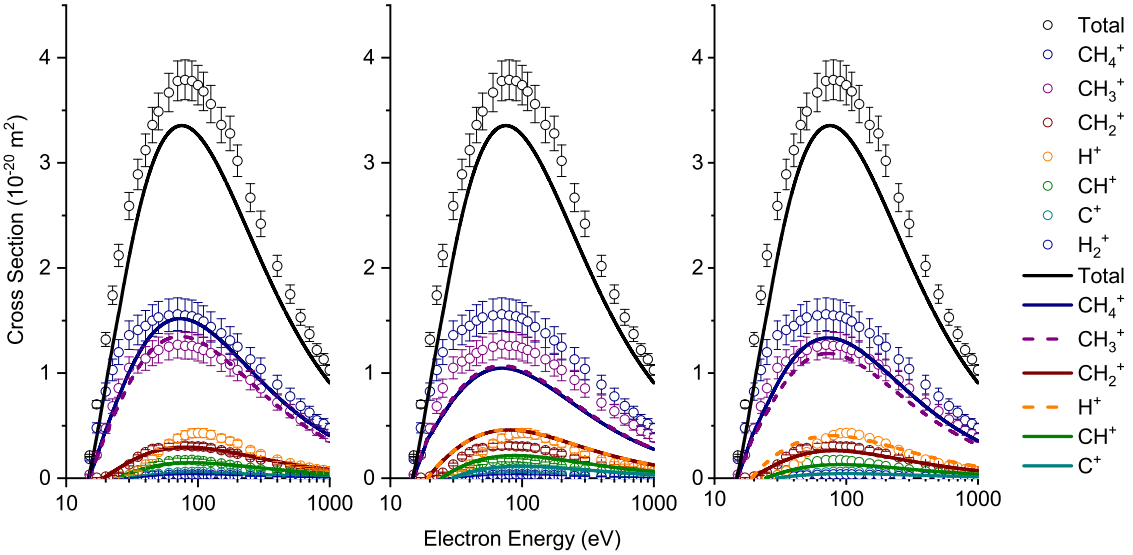

Figure 1. Total and partial ionisation cross sections of CH_4. The circle data points are absolute experimental values by Song *et al* [44]. The solid and dash curves are from this work. The left figure uses the MSD method, the centre figure uses Huber's method and the right figure uses the hybrid method.

shifted so that all fragmentation energies were relative to the Koopmans' theorem IP. The formation of the parent ion was equal to Koopmans' theorem IP.

4. Results and discussion

Three series of molecules were studied, including CH_4, CF_4 and CCl_4 making the CX_4 series, SiH_4 and $SiCl_4$ making the SiX_4 series and finally NH_3 and PH_3 making the XH_3 series. Cross sections are presented up to the highest experimental energy measured. In cases where the data points are larger than the experimental error, no error bars are shown.

4.1. Methane cross sections

A more in-depth study is presented for the first molecule, CH_4. Calculated dissociation thresholds are shown in table 1 and compared to the appearance energies (AE) from experimental data [44].

All calculated thresholds are within the experimental range except for CH_2^+ and H^+. There are multiple pathways that could be used for the formation of these two fragments, and thus the preferred pathway may be different from the lowest energy bond breaking pathway considered here.

The total ionisation cross section of CH_4 is shown in figure 1, as well as partial cross sections calculated using the MSD method, Huber's method and a hybrid method consisting of calculated thresholds where the MSD was not available for a particular fragment ion. The calculated BEB total ionisation cross section is in as good agreement as expected; a similar peak position but a slight underestimation in comparison to the experimental cross section [44]. This underestimation is expected as the BEB method does not fully account for double ionisation channels.

A comparison between the known branching ratios and computed branching ratios assumed to be at a reference energy of 70 eV can be seen in table 2. The percentage errors have the expected trend where those fragments with the highest energy dissociation thresholds have the largest errors.

Table 2. Percentage error of computed branching ratios against known branching ratios at the reference energy.

Energy	CH_4^+	CH_3^+	CH_2^+	CH^+	C^+
70 eV	1.34	1.45	3.88	10.7	18.4

The partial cross sections of the MSD method for CH_4 show a closer match to experimental values than Huber's method. This is evident in the most abundant fragments, CH_4^+ and CH_3^+, lying within the experimental error range; whereas Huber's method significantly underestimates these partial cross sections. The difference between the hybrid model in comparison to the MSD is minimal, as the only change to the model is the inclusion of the fragment H^+ which has a relatively small partial cross section.

In order to be able to compare the models for calculating partial cross sections in more detail, we provide the percentage ion abundances in table 3. These abundances were determined at 30 eV as this energy is high enough that most singly charged fragments will have formed, but below the double ionisation threshold of CH_4. From this table, we can see that the MSD method has the correct ordering of the abundances of the different ion fragments in comparison to the experimental data, with the exception of the very light fragments H^+ and H_2^+. For Huber's method, which uses the dissociation energies to calculate branching ratios, we find an overestimation of the H^+ ion, as well as CH^+ and CH_2^+ ions, and an underestimation of the parent CH_4^+. The overestimation of the fragment H^+ is carried through from Huber's model into the hybrid model. As discussed above, the fragment H^+, as determined from Huber's method, would have many possible pathways of formation, of which only the

Table 3. Percentage abundances for the ion fragments of CH_4 that were determined from the three methods outlined in this work. Abundances were taken at 30 eV and are presented in percentages. Experimental values for CH_4 were taken from the recommendations of Song *et al* [44].

	CH_4						
Fragment	CH_4^+	CH_3^+	CH_2^+	CH^+	H^+	C^+	H_2^+
Experimental	52.51	40.54	5.058	1.127	1.108	0.1197	0.0579
MSD	47.83	42.70	7.281	2.115	0.000	0.0690	0.000
Huber's	35.56	36.49	12.18	3.352	12.26	0.1728	0.000
Hybrid	42.61	38.04	6.486	1.884	10.92	0.0615	0.000

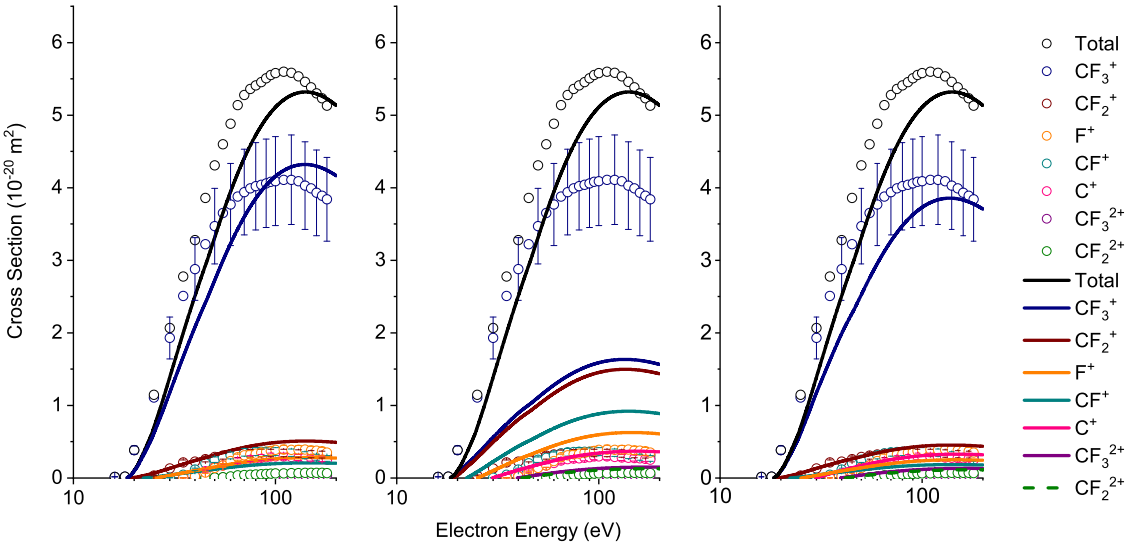

Figure 2. Total and partial ionisation cross sections of CF_4. The circle data points are absolute experimental values by Bonham [45]. The solid and dash curves are from this work. The left figure uses the MSD method, the centre figure uses Huber's method and the right figure uses the hybrid method.

lowest energy route is included in the model. This results in an overestimation. The dissociation threshold was approximately 6 eV lower than the experimental appearance energy, resulting in the fragment abundance being larger than the experiment.

4.2. CX_4 *series*

Comparative ionisation cross sections for CF_4 and CCl_4 can be seen in figures 2 and 3 respectively. Similarly to the methane cross sections, for these two molecules the BEB total ionisation cross section agrees well, particularly at low energy in comparison to experimental data for both CF_4 and CCl_4. The position of the peak in the BEB ionisation cross section of CCl_4 is in close agreement with the experiment, and overall the cross sections are again slightly underestimated.

The experimental partial cross sections for the different ion fragments resulting from ionisation of CF_4 were dominated by the CF_3^+ fragment. Figure 2 shows that this is fragment is also the most abundant when partial ionisation cross sections are determined using the MSD method. For partial cross sections calculated using Huber's method this fragment is still the most abundant species, however the height of the cross section is significantly reduced. In contrast, for CCl_4, both Huber and the MSD method give partial cross sections for CCl_3^+ that are similar to the experimental data, with the MSD method slightly overestimating at the peak, and Huber's model slightly underestimating.

Table 4 shows percentage abundances of the fragments resulting from the ionisation of CF_4 and CCl_4 at 30 eV for quantitative comparison of the models for predicting partial ionisation cross sections. In the case of CF_4, most of the dissociation channels are closed, due to the thresholds being higher than 30 eV. The experimental data shows that most of the ionisation products are CF_3^+ at 93.37% and small amounts of CF_2^+ and CF^+. When producing partial cross sections using the MSD method, this result is preserved, as the CF_3^+ fragment is again the most significant contributor to the cross section. With Huber's model, however, because of the similarities in the dissociation thresholds for CF_3^+ and CF_2^+, the partial cross sections for these species are very similar and thus CF_3^+ is significantly underestimated whilst CF_2^+ is significantly overestimated. Furthermore, the fragments CF^+ and F^+ are also overestimated. The experimental appearance energy of F^+ is at 35 eV. This means that F^+ fragment forms between 30 and 35 eV. Due to its relatively light mass, the measurement of F^+

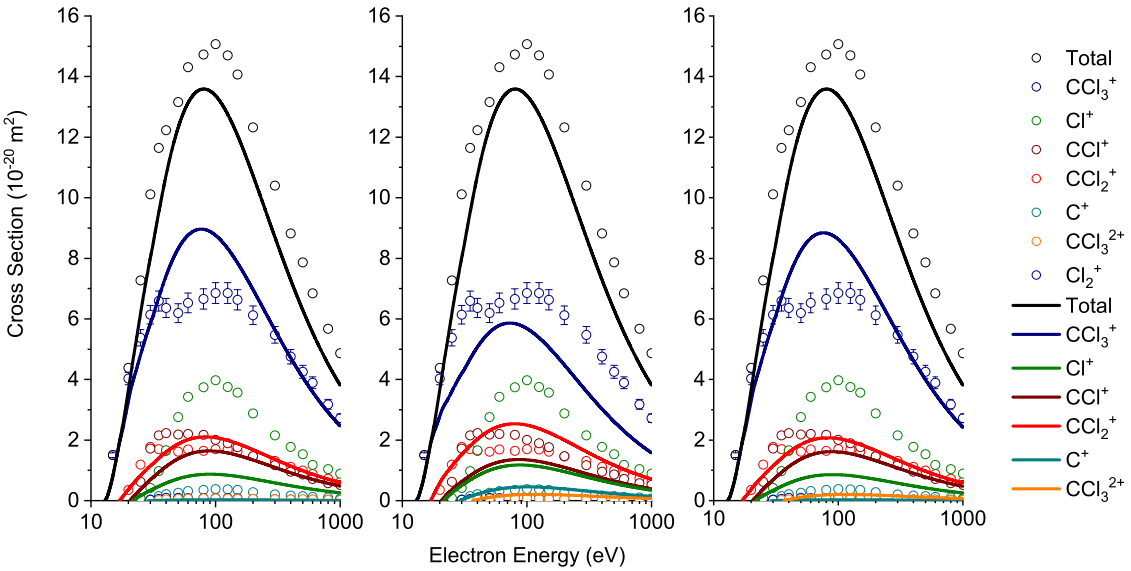

Figure 3. Total and partial ionisation cross sections of CCl_4. The circle data points are absolute experimental values by Lindsay *et al* [46]. The solid and dash curves are from this work. The left figure uses the MSD method, the centre figure uses Huber's method and the right figure uses the hybrid method.

Table 4. Percentage abundances for the fragments of series CX_4 that were determined from the three methods outlined in this work. Abundances were taken at 30 eV and are presented in percentages. Experimental values for CF_4 are by Bonham [45] and values for CCl_4 are by Lindsay *et al* [46].

CF_4							
Fragment	CF_3^+	CF_2^+	CF^+	F^+	C^+	CF_3^{2+}	CF_2^{2+}
Experimental	93.37	6.434	0.1935	0.000	0.000	0.000	0.000
MSD	84.87	9.622	2.921	2.583	0.000	0.000	0.000
Huber's	40.49	35.71	16.28	7.263	0.2569	0.000	0.000
Hybrid	84.66	9.598	2.913	2.577	0.2563	0.000	0.000

CCl_4							
Fragment	CCl_3^+	CCl_2^+	CCl^+	Cl^+	C^+	Cl_2^+	CCl_3^{2+}
Experimental	60.72	17.50	17.01	4.104	0.3758	0.2868	0.000
MSD	72.92	14.27	8.603	4.189	0.02194	0.000	0.000
Huber's	61.06	22.09	9.151	7.280	0.4136	0.000	0.000

should be taken as a lower limit as the ion collection could be incomplete [45]. This could explain why F^+ is included in the models but not the experiment. However, using just dissociation energies to obtain thresholds for appearances of ions has also allows a significant amount of the F^+ and C^+ ions. This leads to two fragments having cross section values that were not detected at 30 eV experimentally. The hybrid method produces abundances which are a reflection of the constituent methods accuracies.

For the final molecule, CCl_4, the MSD method did not include the two smallest fragments, Cl_2^+ and CCl_3^{2+}, of which, the latter has a dissociation threshold higher than 30 eV and so is not observed experimentally at this energy. The abundances of the different fragments compared to the experiment are in reasonable agreement with the largest percentage difference being 12.2% and the relative abundances are preserved. Huber's method gave similar abundances to the MSD method however, this method was also missing the Cl_2^+ fragment due to the fragment selection process. The value at 30 eV for the most abundant species CCl_3^+ lie closer to the experimental value than the MSD method. The hybrid method, despite being used, is not presented in table 4 as the fragment percentages were the same as the MSD method at this energy.

4.3. SiX_4 *series*

The total and partial cross sections for the SiX_4 series can be seen in figures 4 and 5. The shape and magnitude of the BEB total cross sections are similar to the experimental curves. For SiH_4 the total cross section is slightly smaller in magnitude than the experimental error around the peak. However for $SiCl_4$, the total cross section is just within the experimental error at the peak of the cross section.

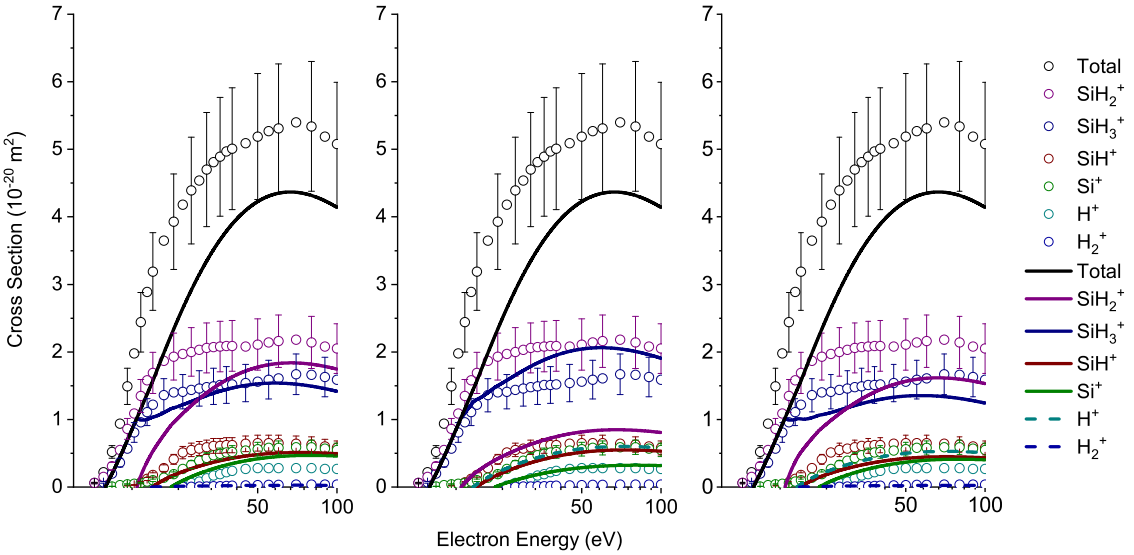

Figure 4. Total and partial ionisation cross sections of SiH_4. The circle data points are absolute experimental values by Basner *et al* [26]. The solid and dash curves are from this work. The left figure uses the MSD method, the centre figure uses Huber's method and the right figure uses the hybrid method.

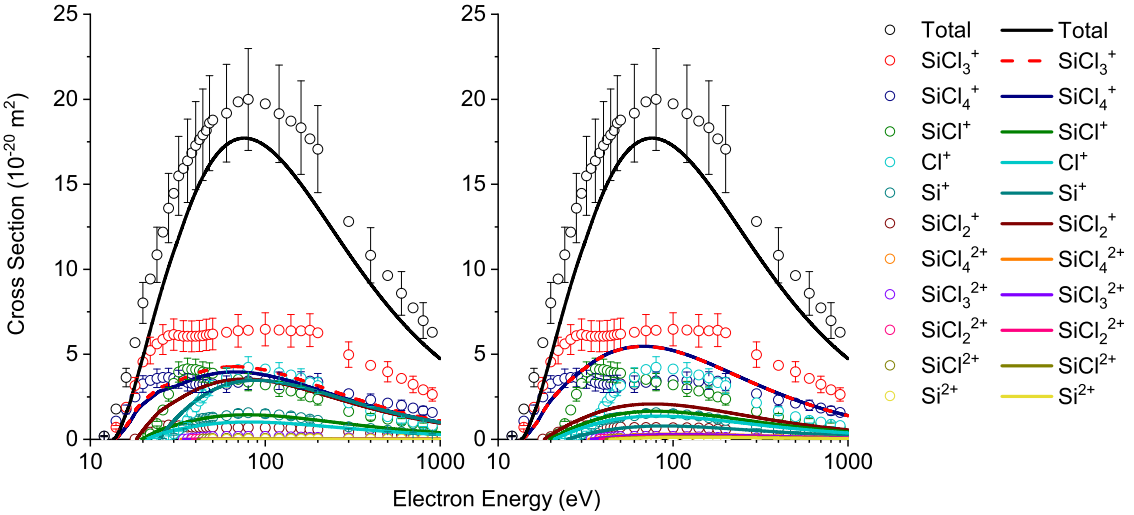

Figure 5. Total and partial ionisation cross sections of $SiCl_4$. The circle data points are absolute experimental values by Basner *et al* [47]. The solid and dash curves are from this work. The left figure uses the MSD method and the right figure uses Huber's method.

It can be seen in figure 4, that the partial cross sections for SiH_4 look the most similar to experimental values when using the MSD (or hybrid) method. The fragment H^+ is missing in the MSD method but not in the hybrid method which is, therefore, the most complete. However, the hybrid method clearly underestimates the three most common fragments: SiH_3^+, SiH_2^+ and SiH^+. The experimental data shows that the most abundant fragment at most energies is SiH_2^+. The MSD method only predicts this fragment as most abundant above 25 eV. In Huber's model the abundance of SiH_2^+ is significantly underestimated, to the extent that SiH_3^+ is predicted to be the most abundant ion for all energies.

For the partial cross sections of $SiCl_4$, it is less clear from figure 5 which method replicates the experimental values the best. Both the MSD method and Huber's model predict near identical abundances of $SiCl_3^+$ and $SiCl_4^+$, however the experimental data shows that $SiCl_3^+$ should be the dominant fragment ion. The values of the partial cross sections at the peak show that Huber's method is in slightly closer agreement with the experimental data for the most dominant ion.

As with the CX_4 series, a table containing the fragment abundances at 30 eV can be used to evaluate the accuracy of the partial cross sections determined using each method. This table is shown as table 5.

For the molecule SiH_4, the MSD method produces results that are generally closer to the experimental results, in terms of both the order of fragment abundance and of the magnitude than Huber's model. The significant exception is SiH_2^+ which is overestimated by the experiment by around 10%. As a result, the other fragments are slightly underestimated.

Table 5. Percentage abundances for the fragments of series SiX_4 that were determined from the three methods outlined in this work. Abundances were taken at 30 eV and are presented in percentages. Experimental values for SiH_4 are by Basner *et al* [26] and values for $SiCl_4$ are by Basner *et al* [47].

SiH_4						
Fragment	SiH_2^+	SiH_3^+	SiH^+	Si^+	H^+	H_2^+
Experimental	44.74	32.18	12.56	8.596	1.763	0.1543
MSD	41.56	41.71	9.837	6.369	0.000	0.5210
Huber's	18.77	54.82	10.34	4.292	11.77	0.000
Hybrid	37.18	37.32	8.801	5.698	10.53	0.4661

$SiCl_4$											
Fragment	$SiCl_3^+$	$SiCl_4^+$	$SiCl^+$	$SiCl_2^+$	Cl^+	Si^+	$SiCl_4^{2+}$	$SiCl_3^{2+}$	$SiCl_2^{2+}$	$SiCl^{2+}$	Si^{2+}
Experimental	42.58	24.82	22.74	5.613	2.260	1.984	0.000	0.000	0.000	0.000	0.000
MSD	30.23	28.05	7.333	19.79	4.699	9.907	0.000	0.000	0.000	0.000	0.000
Huber's	36.48	36.57	7.915	10.97	5.942	2.118	0.000	0.000	0.000	0.000	0.000

Huber's method however, as can be seen in figure 4, overestimates the fragment SiH_3^+ and underestimates the fragments SiH_2^+, SiH^+ and Si^+. The fragment H^+ does not match the experimental results well. While the experimental measurement should be taken as a lower limit [26], the Huber model consistently overestimates light fragments as only the lowest energy route is considered. The fragment order of Huber's method is different to the experiment. This poor agreement is reflected in the hybrid method through the inclusion of the H^+ fragment from Huber's method.

The hybrid model was not calculated for $SiCl_4$, as the mass spectrum used in the MSD method contained all fragments detected experimentally. For the ions detected at 30 eV, presented in table 5, the fragment abundance order from both methods is different from the experiment. Both the MSD and Huber's methods have similar abundances for $SiCl_3^+$ and $SiCl_4^+$, whereas the experimental data shows $SiCl_3^+$ should be 1.7 times more abundant than $SiCl_4^+$. Both methods also have the abundance of $SiCl_2^+$ greater than $SiCl^+$ in contrast to the experimental data. Finally, in the MSD method, there is also a significant overestimation of the Si^+ ion abundance.

4.4. XH_3 series

The XH_3 series contains two molecules, NH_3 and PH_3. Placing an ECP on the phosphorus atom in PH_3 has been found [13] to worsen the agreement between the total BEB cross section and the experimental results. Hence, the total cross sections of both molecules in this series were calculated using the cc-pVDZ basis set. For both molecules, the total BEB ionisation cross section were in close agreement with experimental results, as shown in figure 6 for NH_3 and figure 7 for PH_3.

It can be seen in figure 6, that the MSD method for the calculation of partial cross sections for NH_3 seems to agree well with the experiment for the fragments included. Particularly, the MSD method correctly predicts the NH_3^+ parent ion as being the most abundant especially at low electron impact energy. The partial cross section for NH_2, the next most abundant fragment, is also well produced. The MSD method however significantly underestimates the abundance of H^+ ions particularly at intermediate energies. Conversely, Huber's method determined the H^+ fragment abundance to have a reasonably close agreement with the experimental results from around 50 eV, but overestimates it at lower energies. However, Huber's method significantly overestimates the parent ion, and underestimates the contribution of NH_2^+ to the ionisation cross section. In this case, the hybrid method produces partial cross sections for all fragments which could be used as a reasonable first approximation, as the hybrid method benefits from taking the H^+ results from the Huber method.

The experimental partial cross sections for the ionisation of PH_3 shown in figure 7, show similar abundances of PH^+ and the parent ion PH_3^+ at all energies. Both the MSD and Huber's method do not reproduce this result. For both methods the abundance of the parent ion is overestimated, and the abundance of PH^+ is significantly underestimated. As a consequence, the less abundant fragments are also inaccurate.

Table 6 compares the fragment abundances at 30 eV. For both molecules, the experimental measurement of H^+ can be taken as a lower limit as this light fragment would be more energetic and therefore the ion collection could be incomplete [48, 50]. This could explain part of the discrepancies between the experimental and computational results for H^+.

The mass spectrum data used in the MSD method for NH_3 did not include the fragments H_2^+, H^+ or NH_3^{2+}. Excluding these fragments, the MSD method produces partial cross sections which have the same fragment order as the experiment. Huber's method also agrees with the experimental data in fragment abundance order. The computed dissociation threshold indicates that the fragment N^+ would not have formed at 30 eV, however, this fragment was detected experimentally. Furthermore, Huber's method does not include the fragment H_2^+ due to the fragment selection process.

Of the experimentally detected ions from PH_3, the MSD method was missing the fragments H_2^+, H^+, PH_2^{2+} and P^{2+}. The double ions of PH_3^{2+} and PH^{2+} were detected experimentally at 30 eV. The calculated thresholds indicated that these fragment pathways should not be energetically feasible.

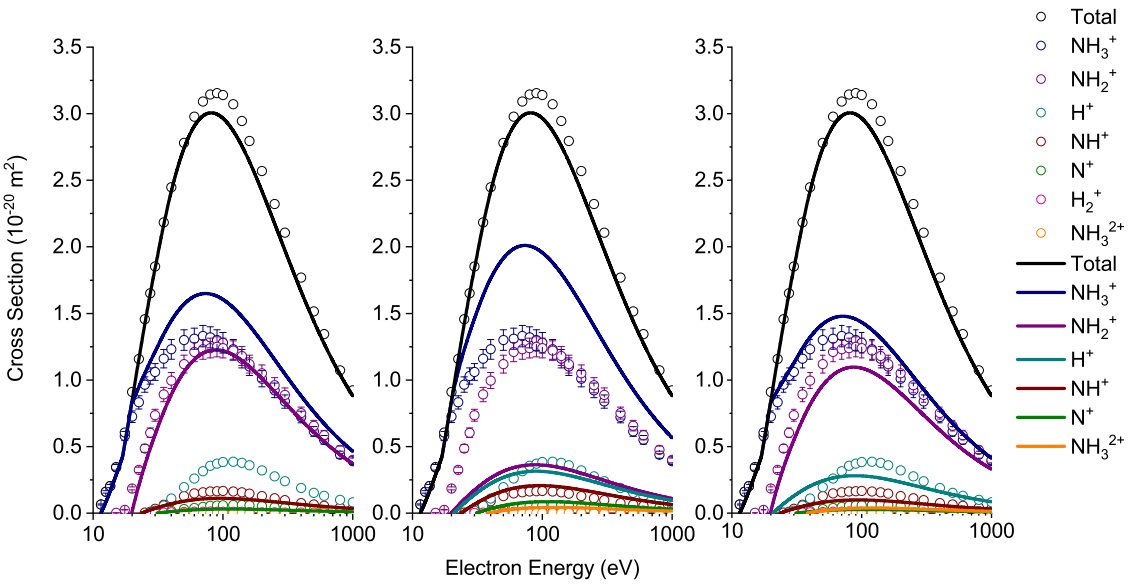

Figure 6. Total and partial ionisation cross sections of NH_3. The circle data points are absolute experimental values by Rejoub *et al* [48]. The solid and dash curves are from this work. The left figure uses the MSD method, the centre figure uses Huber's method and the right figure uses the hybrid method.

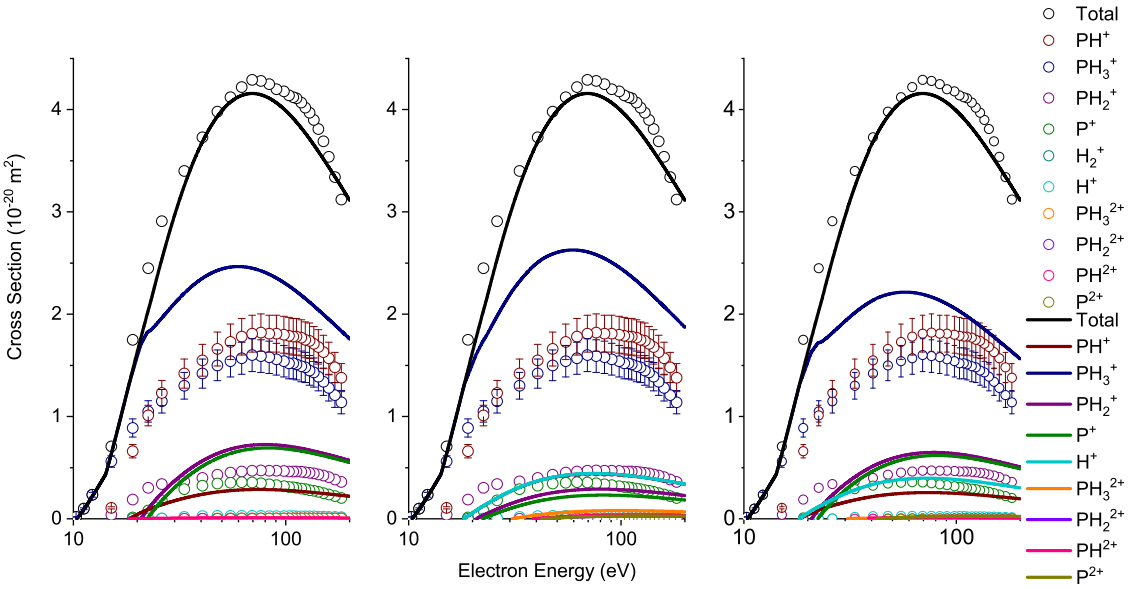

Figure 7. Total and partial ionisation cross sections of PH_3. The circle data points are absolute experimental values by Märk and Egger [49]. The solid and dash curves are from this work. The left figure uses the MSD method, the centre figure uses Huber's method and the right figure uses the hybrid method.

For the remaining fragments PH_2^+ and P^+, the MSD method produces fragment abundances that are close to the experimental results. Huber's method largely underestimates the cross sections due to almost 75% of the partial cross sections being attributed to PH_3^+. Huber's method overestimates the fragments which are missing from the MSD method. This is reflected in the hybrid method. Overall, none of the methods produced fragment magnitudes or fragment abundance orders which were similar to the experimental results. It is possible that, as the models used here do not include all possible electronic processes at all energies, that other processes are particularly prominent in PH_3 and therefore the threshold approximation fails. This could lead to both overestimation and underestimation of fragment abundances.

Table 6. Percentage abundances for the fragments of series XH_3 determined from the three methods outlined in this work. Abundances taken at 30 eV and are presented in percentages. Experimental values for NH_3 are by Rejoub *et al* [48] and values for PH_3 are by Märk and Egger [49].

NH_3							
Fragment	NH_3^+	NH_2^+	NH^+	H^+	N^+	H_2^+	NH_3^{2+}
Experimental	57.24	39.69	1.739	1.026	0.2246	0.07884	0.000
MSD	65.96	32.09	1.955	0.000	0.000	0.000	0.000
Huber's	79.47	9.398	3.596	7.536	0.000	0.000	0.000
Hybrid	61.41	29.87	1.820	6.897	0.000	0.000	0.000

PH_3										
Fragment	PH^+	PH_3^+	PH_2^+	P^+	H^+	H_2^+	PH_3^{2+}	PH^{2+}	PH_2^{2+}	P^{2+}
Experimental	41.78	38.25	10.74	8.503	0.5413	0.1830	0.008 532	0.000 8826	0.000	0.000
MSD	5.950	70.91	12.48	10.29	0.000	0.000	0.1249	0.2344	0.000	0.000
Huber's	8.959	73.80	4.872	3.364	9.006	0.000	0.000	0.000	0.000	0.000
Hybrid	5.459	65.06	11.45	9.443	8.262	0.000	0.1146	0.2151	0.000	0.000

5. Conclusion

Total and partial ionisation cross sections were computed for a range of small, single centred molecules including: CH_4, CF_4 and CCl_4; SiH_4 and $SiCl_4$; NH_3 and PH_3. Total ionisation cross sections were computed using the BEB method, while the partial ionisation cross sections were computed using one semi-empirical method and one fully computational method: the MSD method and Huber's method.

Comparison with experimental results indicate that there is good agreement in the total ionisation cross sections produced using the BEB ionisation model. The shape and position of the maxima agree well with experimental data, although the method overall underestimates the total ionisation cross sections in the case of each of the molecules presented here.

For partial cross sections, the MSD method produces results that are more accurate than Huber's method. However, the MSD method is often missing fragments as they are not included in the mass spectrum, particularly light fragments such as H^+. Huber's method requires no experimental input and therefore could be used as a first approximation when no experimental data is available. A limitation to Huber's method is the formation of fragments outside of the fragment selection process, also resulting in missing fragments. Furthermore, when multiple fragmentation pathways are energetically available, only the lowest energy route is included which results in inaccuracies. It is also clear that dissociation energies alone are insufficient for correctly estimating branching ratios.

A hybrid method can be produced using the MSD method with Huber's method to fill in fragments not included by the MSD method. This can be used to provide a fuller data set but is still limited by the inaccuracies in the methods used to determine the branching ratios.

While this work was being completed Goswami *et al* [51] proposed a method similar to those discussed here. In their method, the BEB cross section is computed for each fragment and the ions are characterized by appearance energy instead of the ionisation energy. Goswami *et al* only considered a single system, methyl alcohol, but their resulting partial cross sections are in good agreement with measurements. Further comparisons between our methods and theirs would be useful.

The plan is to implement fragmentation predictors based on both the MSD and Huber method, or some improved version, in a future version of QEC [38] to allow for the automatic generation of fragmentation patterns alongside the BEB calculation of total electron impact ionisation cross sections which is already available.

Acknowledgments

This work was supported by STFC Grant ST/R005133/1.

Data availability statement

The data that support the findings of this study are openly available at the following URL/DOI: https://doi.org/10.5281/zenodo.5482796.

ORCID iDs

Vincent Graves https://orcid.org/0000-0003-4856-0229
Bridgette Cooper https://orcid.org/0000-0002-4679-3240
Jonathan Tennyson https://orcid.org/0000-0002-4994-5238

References

[1] Itikawa Y 2017 *J. Phys. Chem. Ref. Data* **46** 043103
[2] Montague R G, Harrison M F A and Smith A C H 1984 *J. Phys. B: At. Mol. Phys.* **17** 3295

[3] Kim H-T, Lim J-S, Kim M-S, Oh H-J, Ko D-H, Kim G-D, Shin W-G and Park J-G 2015 *Microelectron. Eng.* **135** 17
[4] Munjal H and Baluja K L 2007 *J. Phys. B: At. Mol. Opt. Phys.* **40** 1713
[5] Asundi R K and Craggs J D 1964 *Proc. Phys. Soc.* **83** 611
[6] Shih M, Lee W-J, Tsai C-H, Tsai P-J and Chen C-Y 2002 *J. Air Waste Manage. Assoc.* **52** 1274
[7] Radoiu M and Hussain S 2009 *J. Hazard. Mater.* **164** 39
[8] Kim Y-K, Hwang W, Weinberger N M, Ali M A and Rudd M E 1997 *J. Chem. Phys.* **106** 1026
[9] Deutsch H, Becker K, Matt S and Märk T D 2000 *Int. J. Mass Spectrom.* **197** 37
[10] Joshipura K N and Antony B K 2001 *Phys. Lett.* A **289** 323
[11] Karwasz G P, Możejko P and Song M-Y 2014 *Int. J. Mass Spectrom.* **365–366** 232
[12] Zhou W, Wilkinson L, Lee J W L, Heathcote D and Vallance C 2019 *Mol. Phys.* **117** 3066
[13] Graves V, Cooper B and Tennyson J 2021 *J. Chem. Phys.* **154** 114104
[14] Bruce M R and Bonham R A 1993 *Int. J. Mass Spectrom. Ion Process.* **123** 97
[15] Bruce M R, Mi L, Sporleder C R and Bonham R A 1994 *J. Phys. B: At. Mol. Opt. Phys.* **27** 5773
[16] Gluch K, Scheier P, Schustereder W, Tepnual T, Feketeova L, Mair C, Matt-Leubner S, Stamatovic A and Märk T D 2003 *Int. J. Mass Spectrom.* **228** 307
[17] King S J and Price S D 2007 *J. Chem. Phys.* **127** 174307
[18] King S J and Price S D 2008 *Int. J. Mass Spectrom.* **277** 84
[19] Endstrasser N, Zappa F, Mauracher A, Bacher A, Feil S, Bohme D K, Scheier P, Probst M and Märk T D 2009 *Int. J. Mass Spectrom.* **280** 65
[20] Ward M D, King S J and Price S D 2011 *J. Chem. Phys.* **134** 024308
[21] Ellis-Gibbings L K, Fortune W G, Cooper B, Tennyson J and Price S D 2021 *Phys. Chem. Chem. Phys.* **23** 11424
[22] Li C, Chin C-H, Zhu T and Hui Zhang J Z 2020 *J. Mol. Struct.* **1217** 128410
[23] Horton L D 1996 *Phys. Scr.* **T65** 175
[24] Poll H U, Winkler C, Margreiter D, Grill V and Märk T D 1992 *Int. J. Mass Spectrom. Ion Process.* **112** 1–17
[25] Seinfeld J H 2008 *Rev. Chem. Eng.* **24** 1–65
[26] Basner R, Schmidt M, Tarnovsky V, Becker K and Deutsch H 1997 *Int. J. Mass Spectrom. Ion Process.* **171** 83
[27] Zhirnov E, Stepanov S, Wang W N, Shreter Y G, Takhin D V and Bochkareva N I 2004 *J. Vac. Sci. Technol.* A **22** 2336
[28] Hamilton J R, Tennyson J, Huang S and Kushner M J 2017 *Plasma Sources Sci. Technol.* **26** 065010
[29] Wallace W E 2016 *NIST Chemistry WebBook, NIST Standard Reference Database Number 69* (Gaithersburg, MD: National Institute of Standards and Technology) p 20899
[30] Irikura K K 2017 *J. Res. Natl. Inst. Stan.* **122** 28
[31] Huber S E, Mauracher A, Süß D, Sukuba I, Urban J, Borodin D and Probst M 2019 *J. Chem. Phys.* **150** 024306
[32] Nishimura H, Huo W M, Ali M A and Kim Y-K 1999 *J. Chem. Phys.* **110** 3811
[33] Janev R K and Reiter D 2004 *Phys. Plasmas* **11** 780
[34] Amorim R A A, Pires W A D, Fernandes A C P, Casagrande T M, Jones D B, Blanco F, García G, Brunger M J and Lopes M C A 2021 *Eur. Phys. J.* D **75** 217
[35] Stein S E 2014 *NIST Standard Reference Database 1A* 2nd edn Gaithersburg MD https://nist.gov/system/files/documents/srd/NIST1aVer22Man.pdf
[36] Huber S E, Seebacher J, Kendl A and Reiter D 2011 *Contrib. Plasma Phys.* **51** 931
[37] Janev R K and Reiter D 2002 *Phys. Plasmas* **9** 4071
[38] Cooper B *et al* 2019 *Atoms* **7** 97
[39] Werner H-J, Knowles P J, Knizia G, Manby F R and Schütz M 2012 *Wiley Interdiscip. Rev. Comput. Mol. Sci.* **2** 242
[40] Dunning T H 1989 *J. Chem. Phys.* **90** 1007
[41] Bergner A, Dolg M, Küchle W, Stoll H and Preuß H 1993 *Mol. Phys.* **80** 1431
[42] Johnson R D 2019 *Computational Chemistry Comparison and Benchmark Database, NIST Standard Reference Database Number 101* http://cccbdb.nist.gov/
[43] Koopmans T 1934 *Physica* **1** 104
[44] Song M-Y, Yoon J-S, Cho H, Itikawa Y, Karwasz G P, Kokoouline V, Nakamura Y and Tennyson J 2015 *J. Phys. Chem. Ref. Data* **44** 023101
[45] Bonham R A 1994 *Jpn. J. Appl. Phys.* **33** 4157
[46] Lindsay B G, McDonald K F, Yu W S, Stebbings R F and Yousif F B 2004 *J. Chem. Phys.* **121** 1350
[47] Basner R, Gutkin M, Mahoney J, Tarnovsky V, Deutsch H and Becker K 2005 *J. Chem. Phys.* **123** 054313
[48] Rejoub R, Lindsay B G and Stebbings R F 2001 *J. Chem. Phys.* **115** 5053
[49] Märk T D and Egger F 1977 *J. Chem. Phys.* **67** 2629
[50] Kumar R 2014 *Chem. Phys. Lett.* **609** 108
[51] Goswami K, Arora A K, Bharadvaja A and Baluja K L 2021 *Eur. Phys. J.* D **75** 228